Available online at www.sciencedirect.com

ScienceDirect

Procedia CIRP 94 (2020) 638–643

www.elsevier.com/locate/procedia

11th CIRP Conference on Photonic Technologies [LANE 2020] on September 7-10, 2020

Statistical analysis of pulsed laser beam welding repair strategies of nickel-base superalloys

Christian Kästner[a], Matthias Neugebauer[a], Klaus Schricker[a], Jean Pierre Bergmann[a,*]

Technische Universität Ilmenau, Production Technology Group, Gustav-Kirchhoff-Platz 2, 98693 Ilmenau, Germany

* Corresponding author. Tel.: +49-3677-69-2981; fax: +49-3677-69-1600. *E-mail address:* jeanpierre.bergmann@tu-ilmenau.de

Abstract

Pulse shaping is a suitable option to adapt energy input and temperature gradients in the base material during filler wire assisted laser beam welding, although the influence on the temperature-depended microstructure and γ'-precipitation strengthening of Nickel-base superalloys as well as the process windows are not sufficiently understood so far. Therefore, the influence of pulse parameters, preheating temperature, hot-wire heating power and wire feeding rate on the deposition process and the resulting macro- and microstructure of similar Nickel-base superalloy joints of Inconel 738 low carbon (IN 738 LC) with Haynes (HS 282) filler are investigated. The statistical analysis of the multidimensional parameter space with respect to the geometric properties of the weld seams (dilution, aspect ratio and wetting angle) and hot-crack formation revealed high reliability and predictability concerning individual choice of suitable parameters in field repair application.

Keywords: nickel-base superalloys; hot-wire technology; pulse shaping; heat management; hot-cracks; statistical analysis; prediction modelling

1. Introduction

Repair welding of γ'-precipitation strengthening nickel-base superalloys is a delicate issue since these materials tend to form hot-cracks due to the occurrence of low-melting phases and thermally induced local mechanical stress, i.e. large temperature gradients between welding zone and base material. Wire assisted pulsed laser beam welding developed as a suitable repair strategy for γ'-precipitation strengthening nickel-base superalloys at moderate temperatures. But, the weldability requires certain technical efforts to avoid/minimize hot-cracks in the heat-affected zone and in the base material as well as distortion and residual stresses if similar γ'-precipitation strengthening filler materials are applied. Pulsed laser beams with durations up to 50 ms and frequencies up to 25 Hz allow the reduction of the average heat input and hence the critical thermally induced stress by sequential melting and solidification of the base and filler material. Further control on the thermal management can be gained by active pulse shaping. The resulting stress gradients can be transformed into crack-free or low-crack regimes [1,2]. The low productivity, i.e. the low welding speed and/or wire melting deposition rate, is the reason for the actually limited application, preferably for industrial repair of individual damages of e.g. turbine blades. The economic and technological limitations are apparently defined by the locally adapted temperature-time regime and the simultaneous increase of productivity. Although the pulse energy and average power of a laser beam source maybe fully utilized, the melting deposition rate is limited, once by the low build-up rates due to the least required frequency or pulse overlap and once by the opposing behavior of dilution and wetting angle, whereas the hot-cracking tendency increases with a larger melting deposition rates [3]. The strategy to decouple heat sources from the laser beam to the filler or base material may increase the productivity by larger melting deposition rates and/or welding speeds, whereas the dilution of

10.1016/j.procir.2020.09.099

the base material is either retained or even reduced. There are two approaches to decouple heat sources, once from the filler material by applying the hot-wire technology and once from the base material by local or global substrate heating. Hence, in this study, a manifold of parameter combinations was applied to control the heat management and the productivity by pulse energy, pulse shape, hot-wire power, preheating temperature of the base material and wire-feeding rate. To conclude about the correlations of each individual parameter and combinations of them on the weld seam geometry (dilution, aspect ratio and wetting angle) as well as the hot-cracking tendency, an intense statistical analysis of 345 parameter combinations was pursued. Thus, information about reliability and predictability of the welding process, concerning individual choice of suitable parameters in field repair application are revealed.

2. Experimental

Wire assisted laser beam welding was pursued with a Nd:YAG pulsed laser (LASAG SLS 200 CL60 HP, laser optics LASAG LLBK60 HP) with a focus diameter of 400 µm and an incidence angle of 10° to the perpendicular in leading direction. Wire feeding was applied with an Elmotec DVS 1490 ALSTOM at an angle of 20° relative to the substrate in trailing direction. Electrical resistance heating of the filler material was generated by applying a constant current between the substrate (cathode) and the wire-feeder (anode). Preheating of the base material was realised with a conventional heating plate (Typ 11A Harry Gestigkeit). Inert-gas argon 4.6 was supplied at an angle of incidence of 40° relative to the substrate with a flow rate of 10 l/min in leading geometry. Fig. 1 depicts a schematic of the experimental setup. The whole setup was controlled by a CNC 3-axis portal system (ILZ Ilmenau Laserportal). Welding speed and pulse frequency were held constant at 0.9 mm/s and 7 Hz, respectively. The wire-feeding rate was varied to 1 mm/s, 2 mm/s and 4 mm/s. The pulse energy ranged from 13 J to 27 J, depending on pulse peak power and pulse shape (PS), see table 1. The cross-marked cells represent non-applicable pulse energies due to the limited average power of the laser beam source. Three pulse shapes were investigated, as shown in Fig. 2. Related temperature profiles from pyrometer (Kleiber KGA 840-LO) measurements are depicted as well.

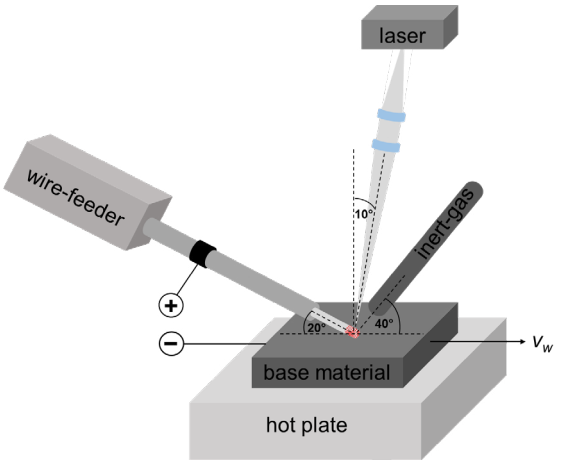

Fig. 1. Schematic of the Experimental setup.

Table 1. Pulse energy as function of pulse shape and pulse peak power.

	pulse energy (*J*)		
pulse peak power (*W*)	PS 1	PS 2	PS 3
800	16.9	14.9	12.9
900	18.9	16.6	14.4
1000	20.9	18.3	15.9
1100	23.3	20.4	17.6
1200	25.3	22.2	19.2
1300	27.2	23.9	20.6
1400	×	25.6	22.1
1500	×	27.3	23.6
1600	×	×	25.2
1700	×	×	26.7

The hot-wire power P_{hw} was varied in four steps, i.e. 0 %, 40 %, 70 % and 100 % of the maximum hot-wire power P_{hw}^{max} = 12 W, yielding 0 W, 5 W, 8 W and 12 W. P_{hw}^{max} was preliminary determined to yield 900°C at the wire tip to obtain high energy input, but certain stiffness of the wire for effective feeding. The base material temperature was varied from room temperature to 430°C in four steps, i.e. room temperature as well as 40 %, 70 % and 100 % of the maximum applicable temperature T_{bm}^{max} = 430°C, yielding 23°C, 172°C, 301°C and 430°C. T_{bm}^{max} was the technical limitation of the heating plate.

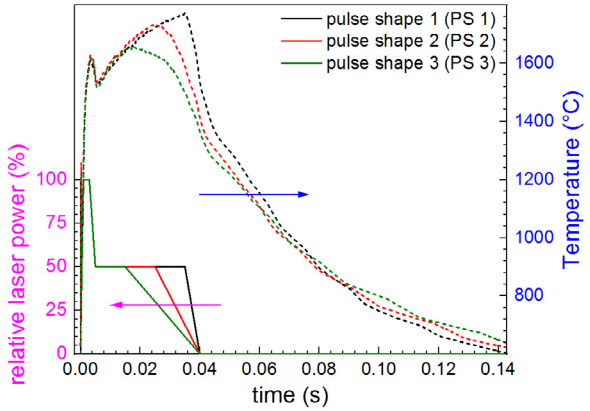

Fig. 2. Applied pulse shapes and exemplary temperature profiles.

The effective heating powers in the base material P_{bm}^{eff} and the hot-wire P_{hw}^{eff}, deposited in the welding zone, can be assumed as follows:

$$P_{bm}^{eff} = 4\rho v_w D_p W c_p \Delta T \quad (1) \qquad P_{hw}^{eff} = \frac{l_{tip}}{l_{wire}} \frac{v_f}{v_w} P_{hw} \quad (2)$$

whereas ρ and c_p are the density and heat capacity of the base material, respectively, D_p the depth of penetration (typically assumed to be 0.5 mm) and W the weld seam width (typically assumed to be 1 mm), ΔT the difference between applied temperature and room temperature, l_{tip} the active heat input length (equal to the laser spot diameter of 400 µm), l_{wire} the totally heated free wire length, v_f the wire-feeding rate and v_w the welding speed. The factor 4 in eq. (1) results from the assumption that the active heating zone dimension is two times the weld seam width W and two times the depth of penetration D_p. The assumptions of the base material preheating are in

accordance to Ref. [3]. The resulting base material preheating powers and thermophysical properties are shown in table 2, corresponding to the applied preheating temperatures of the base material. The thermophysical properties are interpolated from Ref. [4].

Table 2. Thermophysical properties and base material preheating powers.

temperature (°C)	density (kg/m^3)	heat capacity ($J/(kgK)$)	heating power (W)
23	8177	450.0	0.00
172	8133	481.5	1.05
301	8091	506.7	2.05
430	8047	530.2	3.13

The effective hot-wire heating powers are shown in table 3, corresponding to the wire-feeding rate and applied hot-wire power.

Table 3. Hot-wire heating powers for wire-feeding rates of 1, 2 and 4 mm/s.

hot-wire power (W)	effective hot-wire power (W)		
	1 mm/s	2 mm/s	4 mm/s
0	0.00	0.00	0.00
5	0.14	0.28	0.57
8	0.25	0.50	1.00
12	0.36	0.71	1.42

The manufactured weld seams were examined by means of metallographic micrographs with regard to hot-cracking and seam geometry, i.e. dilution D, aspect ratio A and wetting angle Θ. The definition of the geometrical command variables is as follows, in accordance to Ref. [5]:

$$D = \frac{A_p}{A_s + A_p} \cdot 100\% \quad (3) \qquad A = \frac{H}{W} \quad (4) \qquad \Theta = \frac{\Theta_1 + \Theta_2}{2} \quad (5)$$

The results were statistically analyzed with Minitab®, aiming on the extraction of correlations between the input parameters - pulse energy, pulse shape, base material preheating, hot-wire power and wire-feeding rate - and the command variables - dilution, aspect ratio and wetting angle - and finally the deduction of regression functions to predict input parameter sets for aimed command variables [6]. A reasonable statistical significance of the predictors was assured by totally 345 different parameter sets, each backed up by four samples.

Materials under investigation were IN 738 LC as base material and hot-wire with 400 µm diameter of HS 282 as filler material.

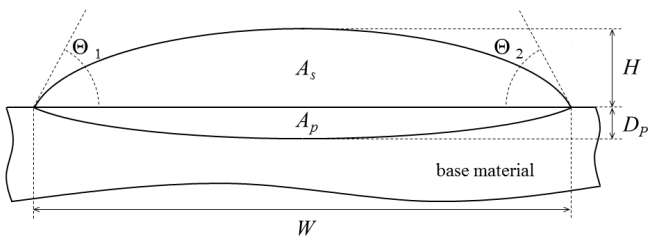

Fig. 3. Schematic of the weld seam geometry and the relevant measurands.

3. Results and Discussion

The interaction between the input parameters and their impact on the geometrical command variables was investigated with about 1,400 micrographs, surveyed and statistically analyzed. The regression function was calculated for each command variable and allowed a statistical optimization of the input parameters to yield command variable sets with certain weighting of each command variable for individual purpose. The input parameters entered linear and bifactorial (square of one parameter or product of two parameters) into the regression functions. The strength of influence of each input parameter in the regression function is represented by the Pareto chart.

The generation and optimization of the regression functions bases on the Anderson-Darling statistics [6,7], which calculates the p-value for the goodness-of-fit, which is used to determine which distribution fits the data for its best. Usually, the p-value or significance level is about 0.05, which means that p-values below 0.05 do not follow significantly any statistics or better to say, the statistic is not trustworthy. P-values larger than 0.05 mean a trustworthy statistic and hence reliable regression functions, whereas the significance is as larger the p-value [8].

Fig. 4 depicts the Pareto charts for the best-fit regression functions of dilution, aspect ratio and wetting angle. The abscissa of the Pareto chart represents the intensity how the different input parameters enter the regression. The ordinate shows the input parameters and combinations of them, sorted by strength from top to bottom.

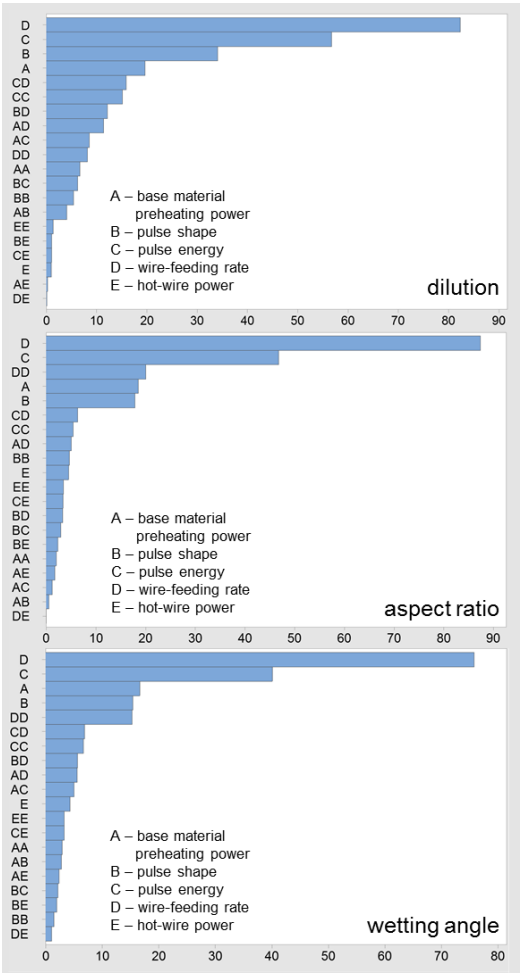

Fig. 4. Pareto charts for the best-fit regression functions.

The Pareto charts reveal the strongest influence of the wire-feeding rate and the pulse energy for all command variables. The influence of pulse shape and base material preheating power is reduced whereas the hot-wire power is subordinate. Also, the factorial terms do not significantly affect the command variables. The obtained p-values of the regression functions of dilution, aspect ratio and wetting angle are 0.072, 0.021 and 0.243, respectively. Hence the regression functions of dilution and wetting angle are trustworthy and the data is subjected to a Gaussian distribution. In contrast, the low p-value of the aspect ratio reveals no significant statistical correlation between the input parameters and the command variable.

The functional correlation between the input parameters and the command variables is represented by the main effects diagram in Fig. 5, which depicts more clearly the findings from the Pareto charts. The steepness of the graphs represents the intensity of impact. The wetting angle and the aspect ratio show nearly the same functional dependency of the individual input parameters. The dilution shows a nearly inverse behavior compared to the wetting angle and the aspect ratio, respectively.

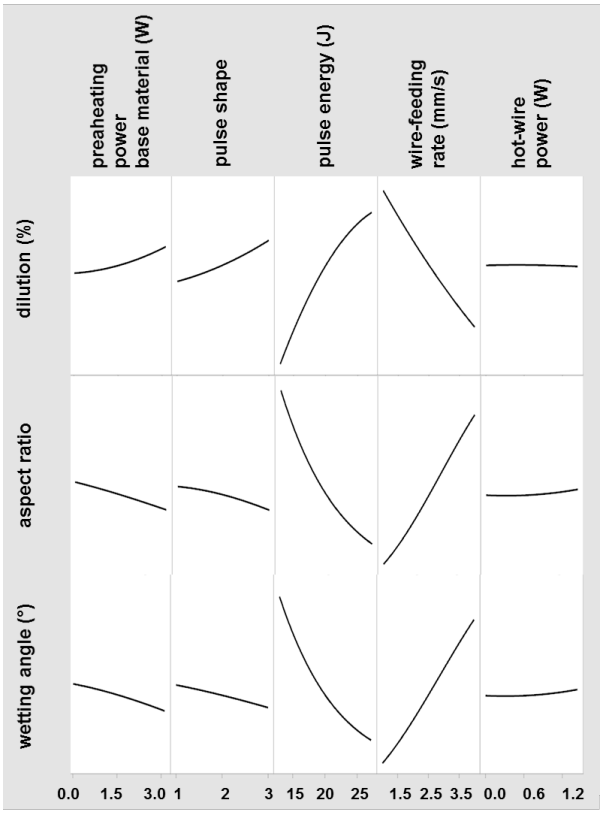

Fig. 5. Main effects diagram.

How the main parental input parameters pulse energy and wire-feeding rate influence the geometry of the weld seam is depicted in Fig. 6. Micrographs of weld seams prepared with 430°C base material preheating temperature and 0 W hot-wire power are exemplarily shown. The top panel (a) shows the micrographs for pulse shape 1 and the bottom panel (b) shows the micrographs for pulse shape 3. The comparison of pulse shape 1 and pulse shape 3 demonstrates the larger dilution and weld penetration for pulse shape 3. This can be explained by the different transient laser beam power distribution for the same pulse energy, compare table 1. The longer ramp-down time of pulse shape 3 leads to a displacement of the laser beam power from the ramp-down region to the pulse peak and the pulse plateau to hold the pulse energy constant. The larger pulse peak power and pulse plateau power leads to a deeper penetration of the laser beam into the base material. On the other hand, whilst increasing the pulse energy leads to larger dilution, clearly visible by the increasing weld penetration, the increasing wire-feeding rate leads to a displacement of the laser pulse energy from the base material into the filler material, which results in decreasing dilution and weld penetration. Hence the energy input in the base material may be reduced as well as the thermal stress, which potentially avoids the hot-crack formation. Additionally, the increasing deposition is a further benefit for repair welding.

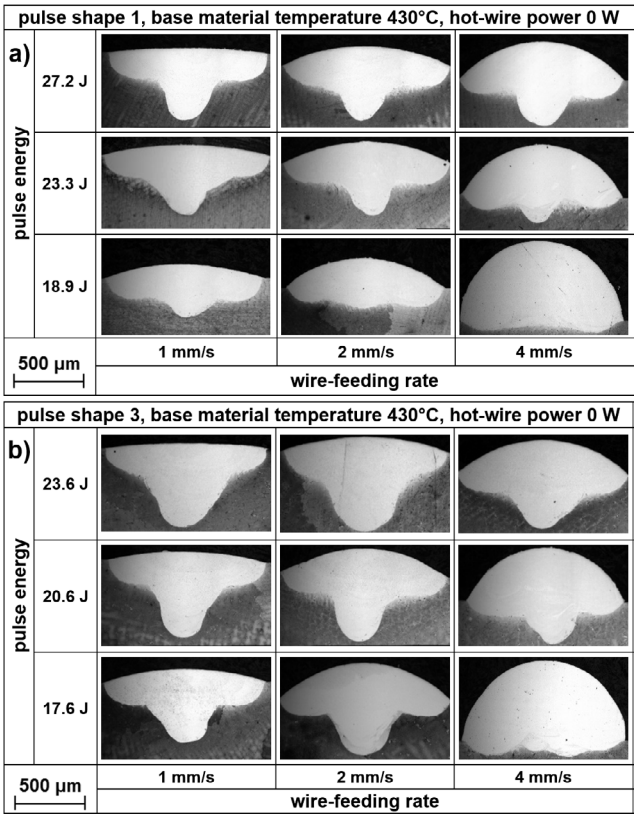

Fig. 6. Micrographs of weld seams.

To represent the subordinate effect of the hot-wire power on the geometry of the weld seams, Fig. 7 depicts the micrographs exemplarily for pulse shape 2, a wire-feeding rate of 1 mm/s and 430°C base material preheating temperature.

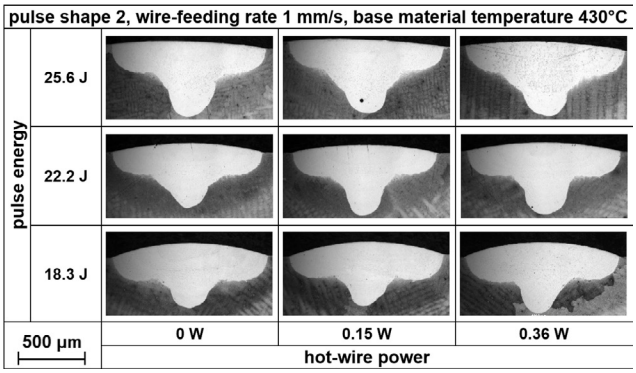

Fig. 7. Micrographs of weld seams.

No effect of the hot-wire power can be observed from the micrographs, which is comparable for pulse shape 1 and 3 (not shown in here). The same effect of larger dilution and weld penetration with increasing laser pulse energy is observed.

To demonstrate the influence of the base material preheating temperature, Fig. 8 exemplarily depicts the micrographs of weld seams generated with pulse shape 3, a wire-feeding rate of 2 mm/s and a hot-wire power of 0 W. Significant differences cannot be observed by eye for the different preheating temperatures of the base material. Nevertheless, the statistical analysis revealed a somewhat similar impact on the weld seam geometry as the pulse shape.

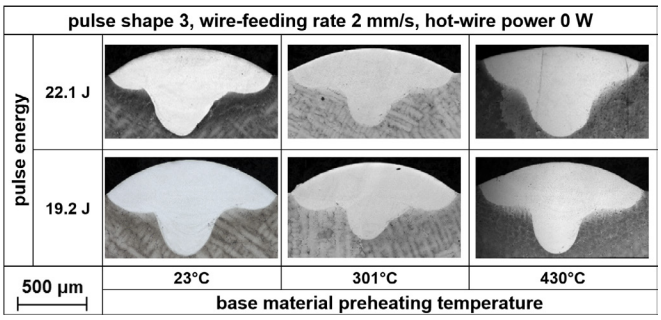

Fig. 8. Micrographs of weld seams.

A further aspect of the statistical analysis, i.e. the extraction of regression functions, is to predict input parameter sets for the generation of specific weld seam geometries. Therefore, the regression functions can be used to calculate the input parameters to yield weld seams with certain dilution, aspect ratio and wetting angle in desirable weighting of each command variable. This combined desirability is shown in Fig. 9 for the case of minimizing the dilution and wetting angle and maximizing the aspect ratio at the same time, which would be the optimum to yield a most desirable weld seam geometry for build-up welding. The x-, y- and z-axis of the diagram represent the weight of the command variables, dilution, aspect ratio and wetting angle, respectively. The color code of the surface represents the combined desirability.

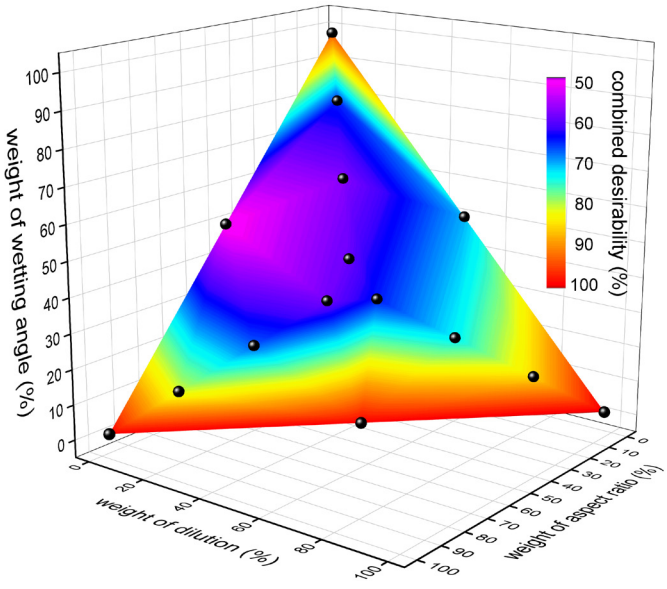

Fig. 9. Combined desirability.

It is obvious that indeed the desirability is 100 % if only one command variable is optimized, but also every possible weight combination of dilution and aspect ratio delivers about 100 % combined desirability if the wetting angle is not taken into account. If all three command variables have to be optimized at the same time the combined desirability reduces at least to 52 %, but it is evident that the wetting angle generally shows a strong impact on the combined desirability. Hence dilution and aspect ratio are well compatible for all weightings, whereas dilution and wetting angle as well as aspect ratio and wetting angle are only well compatible for weightings far away from equality.

How the main effects and the resulted combined desirability are affected by the weighted optimization, is shown in Fig. 10 for a weight distribution of 49.5 / 1 / 49.5 (dilution / aspect ratio / wetting angle), whereas the dilution and wetting angle had to be minimized and the aspect ratio had to be maximized for optimal repair welding conditions.

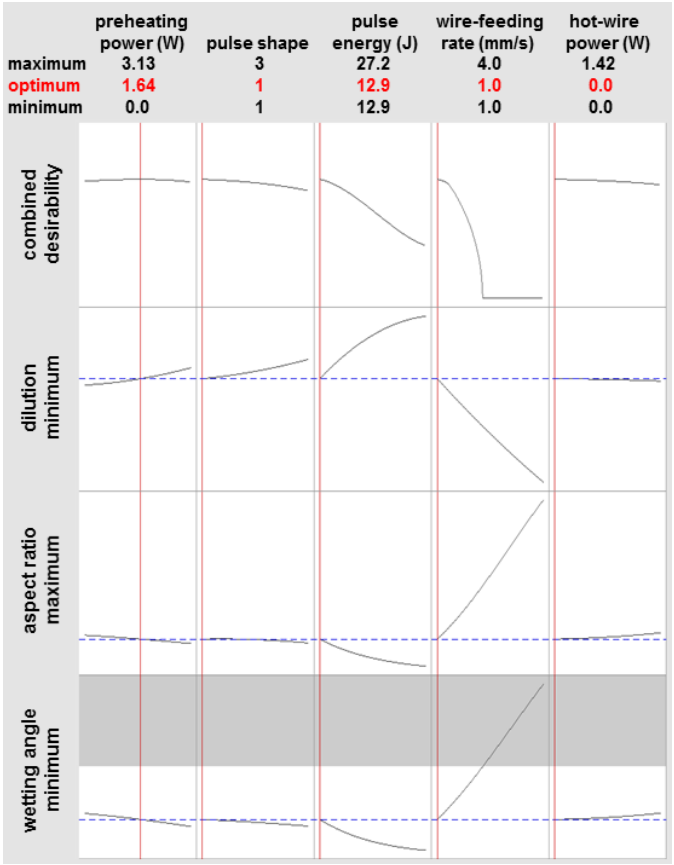

Fig. 10. Optimization for 49.5 / 1 / 49.5 (dilution/aspect ratio/wetting angle).

The optimum values (red) are the values, where the maximum combined desirability is yielded with respect to the aimed optimization ratio. The minimum and maximum values represent the data range of the complete experimental data set, which is optimized. The blue dashed lines indicate the resulted optimized value for each command variable. The red solid lines mark the optimized values of the input parameters. The graphs for dilution, aspect ratio and wetting angle are equal to Fig. 4. It is obvious that all optimal values, except the base material preheating power, are located at the edge of the dataset, which means certain space to improve the predictability of the model by increasing the input parameter range beyond this limit, at

least from a mathematical point of view. However, the expansion of the base dataset is physically limited since the values cannot be smaller than zero like the hot-wire power or even zero like the wire-feeding rate. Even pulse shape 1 is close to a pulse ramp down time of zero, that only the pulse energy leaves realistic space for improvement in this special case of optimization. At this point, the reader's attention is drawn to table 4, where various examples of weighting ratios and the resulting optimal input parameters are tabulated. Based on the combined desirability, depicted in Fig. 8, table 4 shows the corresponding input parameters after optimization, that have to be applied to yield the desired command variables with respect to their weights. This data demonstrates that the optimal values are most likely located far away from the edge of the data set, which means that the base dataset is almost in the optimal range.

Table 4. Weight of command variables and their optimized input parameters.

weight of command variable			optimized input parameters				
dilution (%)	aspect ratio (%)	wetting angle (%)	heating power (W)	pulse shape	pulse energy (J)	wire-feeding (mm/s)	hot-wire power (W)
80.0	10.0	10.0	0.63	1.00	23.48	3.70	0.00
60.0	20.0	20.0	0.00	1.00	12.90	1.09	0.40
40.0	30.0	30.0	2.97	1.06	12.90	1.61	0.35
30.0	40.0	30.0	0.00	1.18	25.47	3.85	0.00
20.0	60.0	20.0	3.13	2.84	12.90	2.45	0.23
10.0	80.0	10.0	3.13	2.98	12.90	2.79	0.03
30.0	30.0	40.0	3.13	1.48	12.90	1.67	0.09
20.0	20.0	60.0	3.13	1.44	12.90	1.12	0.09
10.0	10.0	80.0	3.13	1.30	16.22	1.00	0.11
49.5	49.5	1.00	2.70	3.00	13.62	2.87	0.04
98.0	1.00	1.00	0.51	1.00	23.55	3.69	0.00
49.5	1.00	49.5	1.64	1.00	12.90	1.00	0.00
1.00	98.0	1.00	2.70	3.00	13.62	2.87	0.04
1.00	49.5	49.5	3.13	2.62	12.90	1.73	0.33
1.00	1.00	98.0	3.13	1.06	27.20	1.00	0.29

Finally, the reliability of the regression functions has to be proven in further experiments by applying the optimized values and compare the predicted weld seam geometries with the real weld seam geometries.

4. Conclusion

A valuable method to evaluate a multi-parameter welding process was presented. The statistical analysis of the input parameters with respect to the geometry of the built-up weld seams allowed the extraction of regression functions to mathematically describe the interaction between the input parameters and their impact on the command variables. The regression functions are polynomials of linear and bifactorial terms of the input parameters and allow the prediction of input parameters to achieve certain command variables. Especially the simultaneous optimization of more than one command variable is possible, whereas the geometry of the weld seam can be predicted in different weightings of these variables. The quality of prediction is described by the combined desirability, which becomes as smaller as more command variables at the same time have to be optimized. A correlation between hot-crack formation and the input parameters and hence a regression function could not be found in the current data set. There has to be more data collected to conclude about hot-crack formation by means of a probability distribution.

Nevertheless, further studies have to be pursued to prove the validity of the regression functions. Furthermore, the statistical model shall be extended to further similar materials and also different wire diameters to achieve a more generalized description of the welding process. Finally, the prediction of input parameters of a welding process will allow the applicant to set up the welding process for individual purpose in specific field repair welding scenarios.

Acknowledgements

The authors are grateful for financial support of the AiF Arbeitsgemeinschaft industrieller Forschungsvereinigungen in the frame of the research project 20.023 B / DVS-No. 06.119 of the IGF Industrielle Gemeinschaftsforschung, entitled "Strategien zur Wärmeentkopplung beim gepulsten Laserstrahlauftragschweißen von Nickelbasisbauteilen zur Steigerung der Produktivität".

References

[1] Zhang J, Weckmann DC, Zhou Y, Effects of Temporal pulse Shaping on Cracking Susceptibility of 6061-T6 Aluminum Nd:YAG Laser Welds, Welding Journal 2008, pp. 18-30.
[2] Wilden J, Bergmann JP, Holtz R, Modification of solidification conditions through the set of pulsed Nd:YAG Lasers, XVI. International Symposium on Gas Flow and Chemical Lasers & High Power Lasers Conference 2006.
[3] Bielenin M, Bergmann JP, Abschlussbericht "Prozessstrategie zum Reparieren von Nickelbasisbauteilen mittels Laserstrahl" 2016.
[4] Quested PN, Brooks RF, Chapman L, Morrell R, Youssef Y, Mills KC, Measurement and estimation of thermophysical properties of nickel based superalloys, Materials Science and Technology 2009, 25 (2).
[5] Günther K, Dissertation "Werkstofftechnische Betrachtung zum Heißdraht unterstützten MSG-Auftragschweißen hartstoffverstärkter Verschleiß-schutzlegierungen", Universitätsverlag Ilmenau 2017.
[6] Meyer R, Krueger D, MINITAB Guide to Statistics (2nd. ed.), Prentice Hall PTR 2001.
[7] Anderson TW, Darling DA, Asymptotic Theory of Certain "Goodness of Fit" Criteria Based on Stochastic Processes, Annals of Mathematical Statistics 1952, 23(2),193–212
[7] Greenland S, Senn JS, Rothman KJ, Carlin JB, Poole C, Goodman SN, Altman DG, Statistical tests, P values, confidence intervals, and power: a guide to misinterpretations, Eur J Epidemiol 2016, 31, pp. 337–350.